Precise longitudinal monitoring of corneal change through in vivo confocal microscopy in a rat dry eye disease model

Minjie Chen,[1] Stefanie Seo,[1] Xianni Simmons,[1] Youssef Maroud,[1] Trystin Wong,[1] William Schubert,[2] Samuel C. Yiu[1]

[1]*Wilmer Eye Institute, Johns Hopkins University School of Medicine, Baltimore, MD;* [2]*Bayer AG, Wuppertal, Germany*

Purpose: While lacrimal gland removal is commonly used in animal models to replicate dry eye disease, research into systematically monitoring dry eye disease's longitudinal pathological changes is limited. In vivo confocal microscopy (Heidelberg Retina Tomograph 3 with a Rostock Cornea Module, Heidelberg Engineering Inc., Franklin, MA) can non-invasively reveal corneal histopathological structures. To monitor dry-eye-disease-related changes in corneal structures, we developed a precise monitoring method using in vivo confocal microscopy in a rat double lacrimal gland removal model.
Methods: Five Sprague-Dawley rats (age 8–9 weeks, male) underwent double lacrimal gland removal. Modified Schirmer's tear test, blink tests, and in vivo confocal microscopy images were acquired pre-surgery and at 1, 2, and 4 weeks post-surgery. Three individual stromal nerves were selected per eye as guide images, and images of the corresponding sub-basal nerve plexus area were acquired via volume acquisition. The same area was re-imaged in subsequent weeks.
Results: After double lacrimal gland removal, tear production was reduced by 60%, and the blink rate increased 10 times compared to pre-surgery. Starting from 1 week after surgery, in vivo confocal microscopy showed increased sub-basal nerve plexus nerve fiber density with inflammatory cell infiltration at the sub-basal nerve plexus layer and remained at an elevated level at 2 and 4 weeks post-surgery.
Conclusions: We demonstrated that our precise monitoring method revealed detailed changes in the corneal nerves, the epithelium, and the stroma.

Dry eye disease (DED) is one of the most prevalent chronic ocular diseases today, affecting 5% to 50% of people worldwide, depending on the diagnostic criteria and geographic variations [1-4]. Some common symptoms are eye discomfort, visual disturbance, and ocular pain. Although the biological mechanism of this multifactorial disease is not yet fully understood, recent studies have revealed that the pathological changes seen in DED are associated with neuroinflammation with corneal nerve damage [3,5-9]. It is critical to elucidate corneal changes to understand DED development, disease prognoses, and treatment response evaluations.

In vivo confocal microscopy (IVCM) can produce excellent resolution section images of living tissue at the cellular level. One of the most used IVCM models, the Heidelberg Retina Tomograph 3 with a Rostock Cornea Module (HRT3-RCM) (Heidelberg Engineering Inc., Franklin, MA, USA) generates an image of 400 μm X 400 μm with a spatial resolution of 4 μm. The image displays detailed nerve and cellular structures. With only four to five consecutive Z-axis volume acquisitions, the whole corneal structure, from the anterior epithelium to the endothelium, can be captured within two minutes [1,10-14]. The HRT3-RCM is widely used as a diagnostic tool in ophthalmology to monitor long-term changes in corneal structure [3,11-13,15,16]. However, the field of view of one individual IVCM image is not sufficient to represent the entire corneal condition. In most, if not all, of these previous studies, the cornea has been examined via a random selection of image acquisitions.

The corneal nerve architecture, especially in the sub-basal nerve plexus (SNP) layer, is highly variable, and it changes significantly during disease development. Thus, we developed a novel method to longitudinally monitor changes in the SNP layer using the HRT3-RCM in a rat double lacrimal gland removal (DLGR) model. By using a guide image over a 4-week pre- and post-surgery period, we precisely acquired the same SNP area in each rat by matching its corresponding stromal nerve.

METHODS

Ethical treatment of animals: Five Sprague-Dawley rats (male, age 8–9 weeks, 160–200 g) were purchased from Charles River Laboratories (Wilmington, MA) and maintained in the Johns Hopkins University animal facility. All procedures performed in this study were approved by the Johns Hopkins University Animal Care and Use Committee

Correspondence to: Samuel You, Wilmer Eye Institute, Johns Hopkins University School of Medicine, Baltimore, MD; Phone: (410) 550-2231; FAX: (410) 550-2231; email: syiu2@jhmi.edu

and in compliance with institutional guidelines and the Association for Research in Vision and Ophthalmology Resolution on the Use of Animals in Ophthalmic Research.

Double lacrimal gland removal: The Sprague-Dawley rats were anesthetized by intraperitoneal injection of 75 mg/kg ketamine (VetOne®, MWI, Boise, ID) plus 7.5 mg/kg xylazine hydrochloride (VetOne®, MWI). As shown in Figure 1A, after removing facial hair, a 2-mm incision was carefully made between the temporal lid margin and the zygomatic arch of each rat. The underlying tissue was bluntly separated, exposing the fascia covering the infraorbital lacrimal gland, while avoiding nerves and blood vessels. A small incision was made in the fascia, then the infraorbital gland (#1) was gently pulled out and excised. The incision was sutured with 8–0 Polysorb™ (Ethilon®, Ethicon Inc., Somerville, NJ), and the skin was closed with 5–0 Polysorb™ (Ethilon®, Ethicon Inc.). Then, a 3-mm incision was made just below the earlobe, and the exorbital lacrimal gland (#2) was pulled out and excised along its stem (Figure 1A). Complete removal of both glands was visually confirmed postmortem.

Blink rate test: The rats were placed in an empty cage without lids or bedding and acclimated for 15 min in a quiet room. The number of blinks in both eyes was simultaneously recorded for 5 min using two cell counters. The test was repeated three times in total, and the results were presented as the means of the three repetitions. This test was done at pre-surgery and 1 week, 2 weeks, and 4 weeks post-surgery.

Modified Schirmer's tear test: Tear production was measured using a modified Schirmer's tear test strip [17]. While the rats were under anesthesia, 2-mm-wide strips were cut from regular Schirmer's test strips and placed in the conjunctival fornix of both of each of the rat's eyes for five minutes. The length of the wet area was measured immediately using a digital caliper. This test was done at pre-surgery and 1 week, 2 weeks, and 4 weeks post-surgery.

Cornea fluorescein staining: While the rats were under anesthesia, one drop of 0.25% fluorescein sodium solution (Altaire Pharmaceuticals Inc., Aquebogue, NY) was added into the conjunctival fornix of each rat's eye. The rats' eyes were manually closed twice and washed with 2 ml saline after 1 min. The rats' eye images were acquired by a Phoenix Micron slit lamp (Phoenix-Micron Inc., Bend, OR). This test was done at pre-surgery and 4 weeks post-surgery (Figure 1B).

In vivo confocal microscopy: The rats were anesthetized with ketamine (75 mg/kg, KetaVed®, VEDCO, St. Joseph, MO) and xylazine (5 mg/kg, XylaMed®, Bimeda-MTC, Cambridge, ON, Canada). GenTeal® (Alcon, Fort Worth, TX) was applied
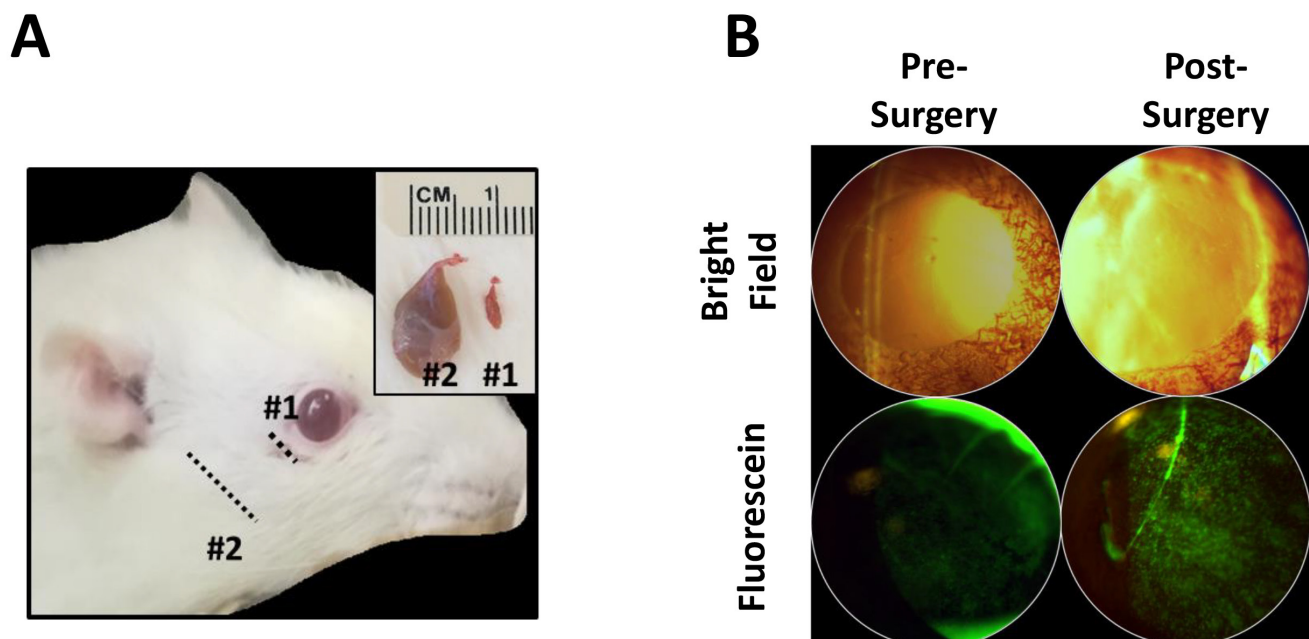

Figure 1. Establishing the dry eye model by double lacrimal gland removal (DLGR). **A**: Left, incision locations of the infraorbital [1] and exorbital [2] lacrimal glands and right, excised lacrimal glands. **B**: Bright-field and fluorescein staining of rat cornea pre- and post-DLGR surgery.

to both eyes to prevent drying. The HRT3-RCM with a modified rodent platform was used to examine all the corneal layers. Image acquisition at zero was uniformly set at the basal cell layer, while the presence of keratocytes indicated the beginning of the anterior stroma. A series of sequential volume acquisitions, typically four to five, were taken from position -10 µm (within the epithelium layer) to around +150 µm (passing the endothelium layer). IVCM images were acquired pre-surgery and at 1, 2, and 4 weeks post-surgery.

Longitudinal IVCM monitoring imaging protocol for DED: To longitudinally monitor corneal changes by IVCM, we modified the HRT3 platform for animal research (Figure 2A). The original chin supporter was removed, and a 3-D platform was mounted on the IVCM table so that we could finely adjust the position of the rats' eyes in the x-y-z axis. The approach used to precisely track corneal changes was to set up guide images during the initial pre-surgery acquisition (Figure 2B). We located the area of interest by identifying a stromal nerve with distinguishing branching architecture at the posterior stromal level, around 70–90 µm to the corneal epithelium basal layer. The whole cornea, including SNP images, was then acquired via 4–5 successive volume acquisitions from the same locations. In the follow-up exam, we found the same stromal nerve by following the same protocol (same animal position, same nerve depth, and same IVCM operator). In this way, the same SNP area could be compared at various time points (Figure 2B,C). We began by recording three different guide images from the stromal nerves in each rat, and in the subsequent acquisitions, approximately two out of three nerve guide images were successfully located at each time point. Each acquisition took 30 min or less for each eye. A representative set of guide images and SNPs pre- and post- surgery are presented in Figure 2C.

Rat cornea nerve architecture by whole mount staining: The rat corneas were harvested right after euthanasia by CO_2 asphyxia. After a 2-h fixation in 10% neutral buffered formalin (Sigma, St. Louis, MO), the corneas were treated with 1.0% Triton X-100 for 2 h (Sigma), followed by blocking with 5% horse serum (Thermo Fisher Scientific, Waltham, MA) and 0.5% Triton X-100 (Sigma) in PBS (Sigma) for 24 h. The corneal nerves were detected by 1:500 mouse anti-tubulin beta III (TUBB III, BioLegend, San Diego, CA), followed by 1:500 FITC-anti-mouse (Thermo Fisher Scientific). Images were then acquired by a Zeiss confocal LSM 700 microscope (Zeiss, Jena, Germany) and processed by ImageJ (NIH, Bethesda, MD).

Statistical data analysis: The current study acts as a proof of concept for using anatomic landmarks to precisely monitor SNP changes. Prior to the surgery, we captured images of three distinct areas in each animal, establishing the baseline. Post-surgery, we continued monitoring the same areas at subsequent time points. Consequently, each animal contributed three sets of data at every time point. The data collected during the baseline phase was used as the internal control for the subsequent post-surgery measurements.

The data are presented as mean ± SD and were acquired at the following time points, as indicated previously: pre-surgery, 1 week post-surgery, 2 weeks post-surgery, and 4 weeks post-surgery. A one-way ANOVA was used to assess differences between groups, and the Student *t* test via Prism9 (GraphPad Software, San Diego, CA) was used to detect statistical differences between groups. Statistical significance was defined as $*p<0.05$, $**p<0.01$, $***p<0.001$.

RESULTS

Dry eye animal model established by DLGR: As shown in Figure 1A, we successfully removed the infraorbital and exorbital lacrimal glands in all five animals without complications. After 4 weeks, the post-surgery eye showed a marked increase in fluorescein staining, indicating typical corneal DED changes (Figure 1B). The blink test, a behavioral readout indicating the eye's dryness and uncomfortableness to the animal, increased from fewer than 1.9 blinks/5 min before surgery to 11.8 blinks/5 min after 1 week post-surgery, reaching 24.7 blinks/5 min after 2 weeks and remaining at 19.5 blinks/5 min after 4 weeks ($***p<0.001$, Figure 3A). Correspondingly, the Schirmer's test showed that tear secretion decreased from 2.5 mm/5 min pre-surgery to 0.93 mm/5 min post-surgery, then stayed at approximately 1 mm/5 min post-surgery without sign of recovery at week 4 ($**p<0.01$, Figure 3B).

Comparison of rat cornea nerve architecture acquired by whole mount staining and IVCM: To compare the nerve structure acquired by IVCM with the corneal true nerve architecture, we stained the rat corneas with TUBB III (BioLegend) and reconstructed the entire corneal nerve map (Figure 4A). We manually matched the IVCM guide images with the whole mount nerve architecture (Figure 4A, blue and red squares) in a small lateral-temporal area of the cornea. Note the concordance of the nerve morphology visible in the cornea whole mount staining and IVCM (Figure 4B, left—whole mount versus right—IVCM), as well as the close spatial localization of the two areas.

Corneal SNP changes during DED development: In the SNP layer, we were able to acquire the relatively thick anterior stromal nerve (Figure 5A, upper panel, red lines), together with the typical thin, parallel-arranged SNP fibers (Figure 4A, upper panel, white lines). We detected 1.72±0.38 SNP

nerves/image pre-surgery. One week after surgery, there were more distinguishable SNP nerves (2.85±0.64 nerves/image) visible, as shown in Figure 4A. At 2 weeks post-surgery, the number of detectable nerve fibers was 3.58±0.32 nerves/image in the same area. The number of detectable nerves was 3.51±0.30 SNP nerves/image at 4 weeks post-surgery. We also noticed that the number of small, highly reflective cells increased from 0.73±0.26 cells/image pre-surgery to 3.04±0.28 cells/image 1 week post-surgery. This was followed up at 3.23±0.54 cells/image at 2 weeks post-surgery and 3.64±0.46 cells/image at 4 weeks post-surgery. There was no significant change in nerve trunk diameter, nerve sprouting, or keratocyte activation in the posterior stroma IVCM (data not shown), where the guide images were acquired (Figure 4A, lower panel, red lines).

DISCUSSION

In this study, we developed a novel method of longitudinally monitoring SNP nerve changes in a rat DED model. This method revealed dynamic changes in SNP nerve density and inflammatory cell infiltration during DED development.

Corneal nerve architecture is not evenly distributed. Stromal nerves stem from the limbal sclera and branch out toward the central cornea, forming an infero-central whorl-like SNP with unmyelinated axons, and they further branch
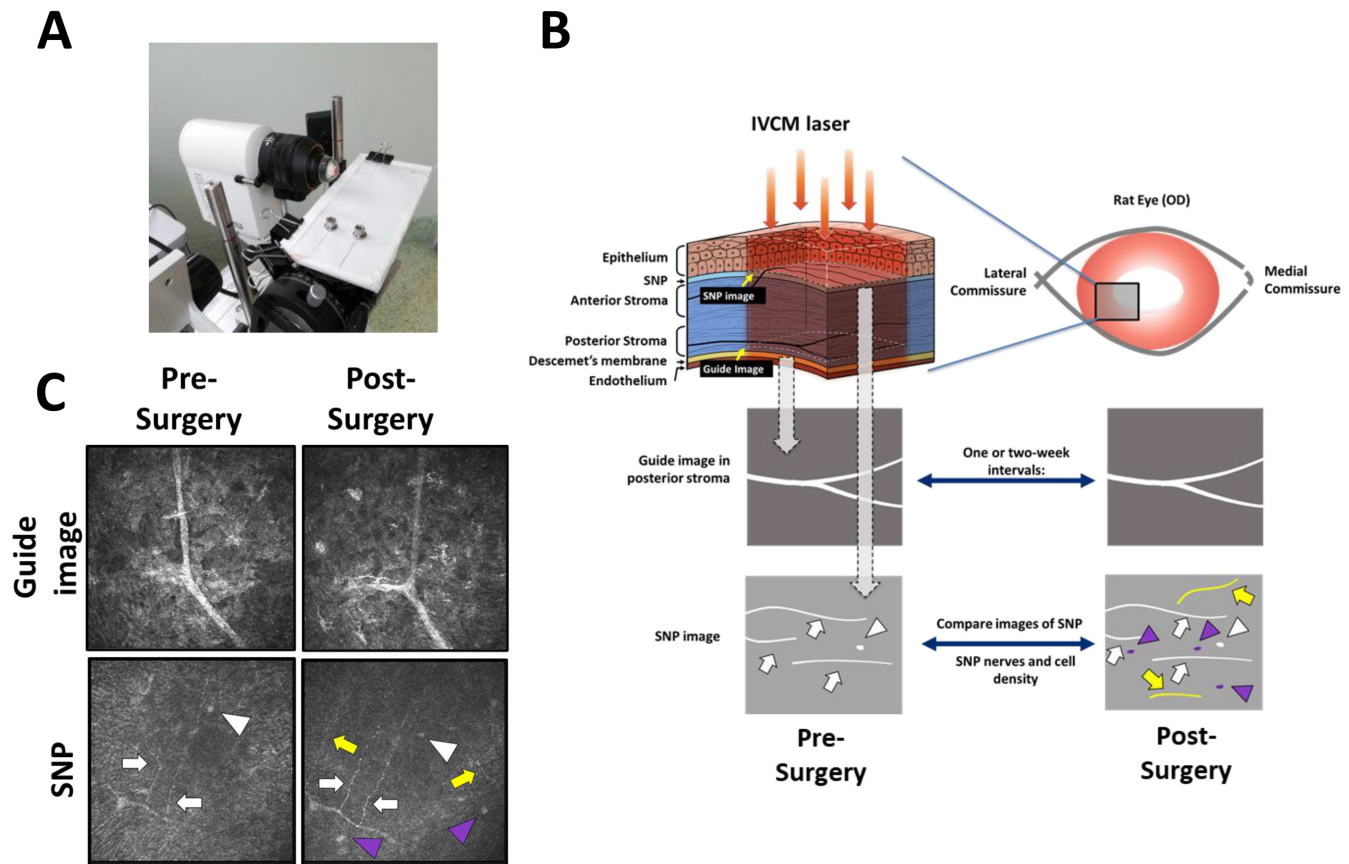

Figure 2. Protocol of longitudinal IVCM monitoring of dry eye development. **A**: Modified HRT3 platform for animal research. **B**: The flowchart of longitudinal IVCM monitoring of dry eye neural changes. Pre-surgery: guide image of the posterior stromal nerve was recorded, and corresponding SNP images were recorded anteriorly through volume acquisition. Post-surgery: The same posterior stromal nerve was located after DLGR, and SNP images were recorded and compared to previous SNP images. Note that the similar morphologies of stromal nerves of guide image and SNPs illustrate that the same corneal area was imaged at different time points. SNP nerves were counted (white/yellow lines with white/yellow arrows), as well as cell infiltration (white/purple dots with white/purple triangle arrows). **C**: A typical set of IVCM images before and after surgery, showing similar morphology to guide images and SNPs. White lines and/or white arrows: SNP nerves detected in both pre- and post-surgery SNPs. Yellow lines and/or yellow arrows: SNP nerves detected only in post-surgery SNPs. White dots and/or white triangles: SNP cells detected in both pre- and post-surgery SNPs. Purple dots and/or purple triangle arrows: SNP cells detected only in post-surgery SNPs.
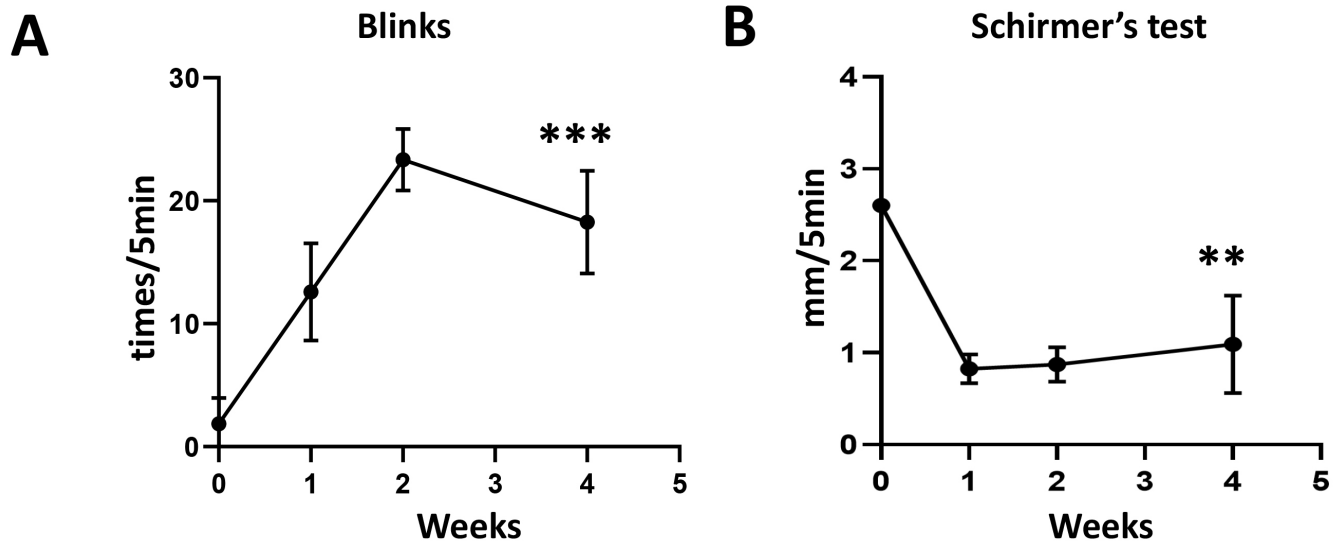
Figure 3. DLGR induced increased blink test and decreased tear production. **A**: Average blink rate increases after DLGR (n=5, ***$p<0.001$, compared to pre-surgery eyes). **B**: Modified Schirmer's test length measurement after 5 min (n=5, **$p<0.01$, compared to pre-surgery eyes). Data are presented as mean±SD.
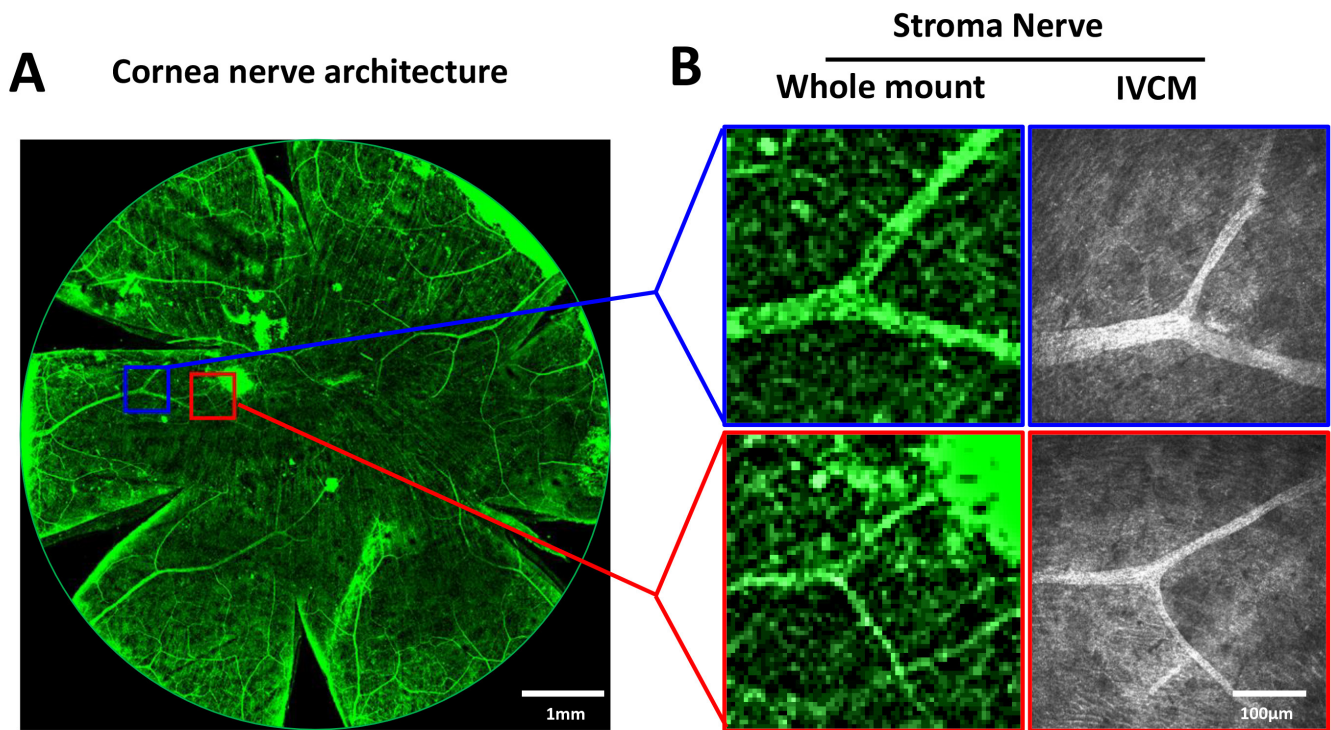

Figure 4. Comparison of whole mount images of rat cornea and IVCM. **A**: Whole mount image of one rat corneal nerve architecture stained with anti-TUBB III acquired by LSM710 and processed by ImageJ. Two guide images of this rat cornea were visually compared with the nerve structure seen in the whole mount (**B** left, enlarged from whole mount; **B** right, IVCM).
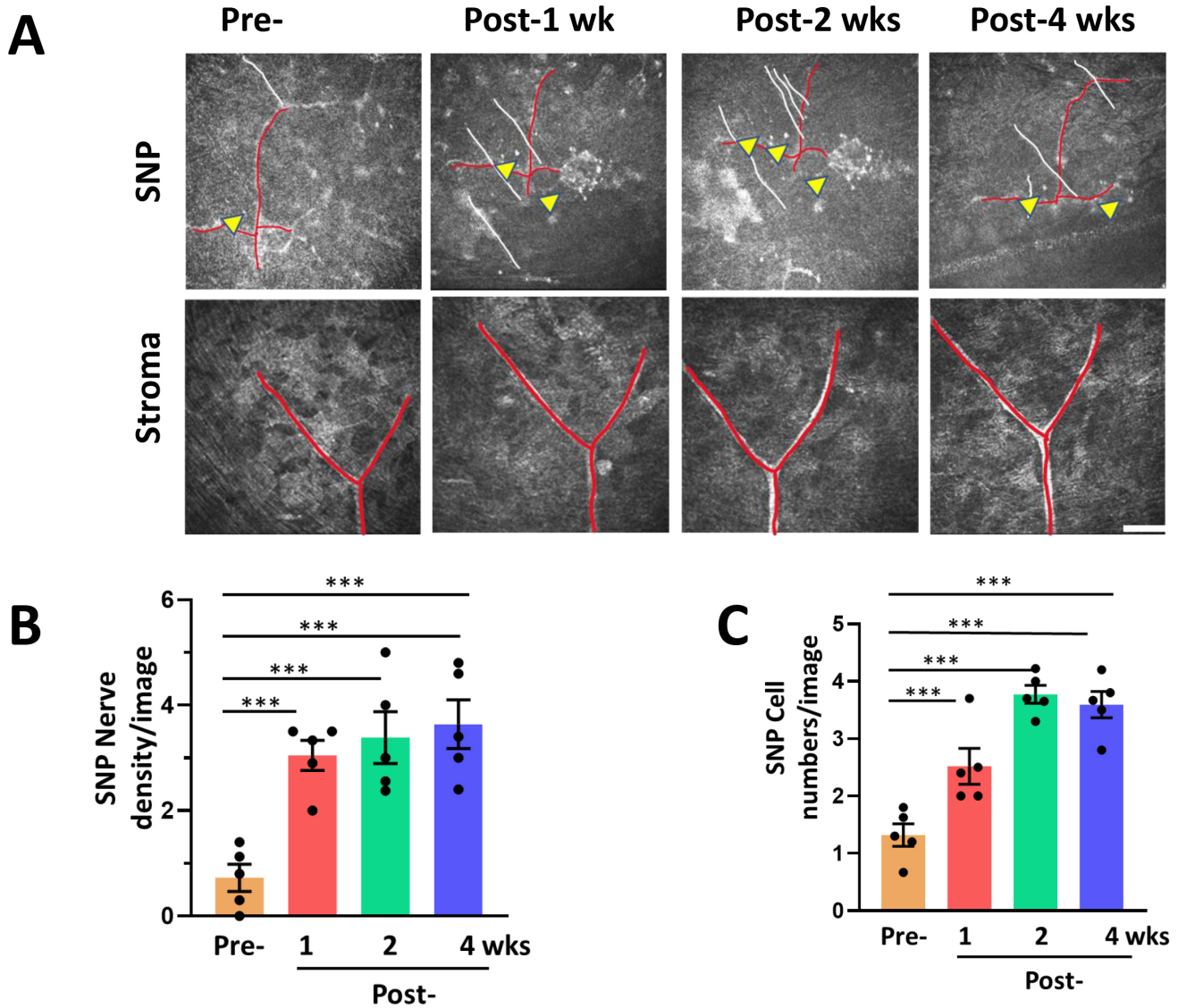
Figure 5. IVCM images of corneal changes after DLGR. **A**: Representative pre-surgery and post-surgery IVCM images at weeks 1, 2, and 4. The guide image (**A**, lower left panel) was acquired from the posterior stromal layer (approximately 70–90 µm) before surgery, and the corresponding SNP image is shown in the upper panel. Note the same morphology of the nerve marked as a red line in both the guide image (**A**, lower panels at various time points) and the SNP (**A**, upper panels at various time points). White lines: detected SNP nerves. Yellow arrow: newly detected inflammatory cells. The quantification of newly detected SNP and inflammatory cells is presented as nerve density/image and cell numbers/image in **B** and **C**, respectively (n=5/group, ***p<0.001, **p<0.01, compared to pre-surgery). Data are presented as mean±SD.

forward as free nerve endings in the epithelial layer [16-20]. The SNP layer is of great interest in IVCM imaging because of its unique nerve fiber distribution and easy-to-identify cell infiltration. But each IVCM image has an area of 400 µm X 400 µm, accounting for 0.2% of the human cornea, or 0.8% of the rat cornea. To obtain more representative images of the corneal SNP, previous studies have acquired up to 20 random areas in one eye [17], which still only covered a small portion

of the cornea. Thus, to interpret IVCM images correctly, it is beneficial to define an anatomic landmark during imaging acquisition. To our knowledge, our study is the first attempt to precisely monitor longitudinal corneal nerve change via IVCM. Our method acquired comparable SNP images (Figure 5A, upper panel), no matter how dramatic the change to SNP layers during disease progression. In our next study, we

would like to compare those images with randomly captured SNP images to better determine the accuracy of this method.

While our current study marks the first described attempt for longitudinally monitoring corneal nerve structure in research animals, similar attempts have been used in human studies, unveiling invaluable insights into the dynamic change of the corneal nerve architecture in healthy and diseased patients. In humans, the center of the cornea SNP forms a unique swirl apex shape, serving as a commonly used anatomic landmark in longitudinal IVCM monitoring. A recently reported longitudinal IVCM study by a modified large-area IVCM is a good demonstration of the importance of precise location for objectively detecting SNP changes. Although the sample size in this previous research was only three healthy participants, the study revealed that the cornea SNP nerve branching point migrated at a speed of 48 μm/week in the 6-week follow-up [21,22]. In another study of three healthy individuals, a 50-min IVCM observation at the same SNP location uncovered immune cell migration at a speed of 1.2 μm/min [23]. Lately, a larger scale study from the same group enrolled 30 participants as healthy controls or ocular allergy patients. This study demonstrated that the allergy patients had altered immune and keratocyte cell morphology compared to the healthy controls, and this alteration was modulated with therapeutic intervention [24]. In line with individualized medicine, longitudinal IVCM monitoring offers a distinct advantage for accurately predicting prognosis and assessing drug responses. However, to harness this advantage to its fullest potential, it is imperative to establish a comprehensive data set encompassing patient profiles and healthy population data. We acknowledge the necessity of incorporating control groups and expanding the sample size for robust testing. These measures are essential for applying the proposed method in translational research involving larger animals and, eventually, human subjects. Meanwhile, it is noted that both these methods (using either the SNP swirl or the deep stroma nerve as the anatomic landmark) are time consuming, and scaling up these methods for a larger number of patients may require innovations in imaging processing, hardware detection, and protocol development.

In our study, fluorescein staining was used primarily to validate the DED rat model, not for quantifying the severity of DED. However, it holds significant relevance if we intend to extend this method to future patient studies. In human DED patients, while the severity of DED is often perceived subjectively according to the ocular surface disease index (OSDI) questionnaire, the Oxford score is a quantitative fluoresceine staining evaluation that measures corneal epithelium damage. It has been reported that corneal SNP density is negatively correlated with the Oxford score in a cross-sectional study [25]. While the methodology we employed here provided longitudinal monitoring of DED development, it would be interesting to correlate changes in nerve density with dry eye severity in the future.

Despite its great promise, our stromal-SNP nerve tracing method using IVCM has clear drawbacks because of its low efficiency. The process of locating the same guide images requires a researcher's IVCM imaging techniques to be highly precise. Memory of the initial position of the rat's eyeball was critical for finding the guide images in follow-up acquisitions. IVCM images can also be easily distorted by acquisition angles or animal breathing. Our method also relies on the visual comparison of the guide images during acquisition, which further decreases efficiency. Considering that the rat corneal surface area is approximately one-quarter the surface area of the human cornea, it would be much more challenging to apply this method for clinical use [19,20]. A newly developed imaging instrument, micro-optical coherence tomography (μOCT), can generate stromal nerve architectures in high-resolution imaging in a significantly shorter scanning time [26]. Meanwhile, developing an imaging comparison algorithm to reduce the guide image matching time is also promising. Combined with hardware and software development, we could achieve a shorter examination time, which makes this concept more feasible for use in ophthalmology clinics.

It is well established that removing the lacrimal gland(s) induces an acute inflammatory response in corneal tissue, showing inflammatory histological changes or detection of inflammatory cells through flow cytometry [17,27-30]. IVCM also provides clear evidence of the neuroinflammatory nature of a surgically induced DED model, such as dendritic cell infiltration in the SNP layer and immune cell increase with activated keratocytes in the stroma [11]. In our study, neuroinflammation, as measured by detectable SNP nerves and inflammatory cell infiltration, peaked between 1 and 2 weeks post-surgery and remained high at 4 weeks post-surgery. The direct comparison of the same IVCM area shows numeric changes to SNP nerve fibers and inflammatory cells in the SNP layer, which provides a quantitative method to measure neuroinflammation. However, the increased numbers of nerve fibers seen in IVCM are unlikely to have resulted from new SNP nerve sprouting. Morphologically, these parallel distributed SNP nerve fibers, as shown in Figure 4A, appeared to be unable to grow full length nerve fibers during this short duration (1 week post-surgery). Here, we speculate that increased SNP density was caused by nerve fiber edema, which increased the diameter of nerve fibers that reached

the detection limit of IVCM. It also has been reported that IVCM normally detected many fewer nerve fibers compared to corneal whole mount staining [31]. In our study, we did not notice significant infiltration of inflammatory cells at the layer of the posterior stroma used for guide images, which is consistent with previous reports that inflammatory cells migrate through the anterior stroma [32]. Additionally, this may be because our DLGR DED animal model was relatively less severe than in other studies, which completely removed the Harderian glands [11]. In our study, we kept the Harderian gland intact, leaving a low level of tear secretion, as shown in Figure 3B.

In various DED animal models or human studies, there has been no conclusive change seen in SNP nerve density. In animal studies, it has been reported that the SNP nerve density is lower in corneal scrapings of mice under dry eye conditions compared to control mice, as well as in air-fan-induced and scopolamine-induced DED mouse models [17,33]. Studies on human patients with clinical DED have not yielded definitive results either. In a meta-analysis of 11 human studies, it was found that most of the studies showed lower nerve density or marginally lower nerve length [25,34-39], though one study reported no change in nerve density [40] and another reported a significant increase [41]. Considering that DED is a chronically developing disease in humans and that DLRG induced acute corneal neuroinflammation within weeks, the long-term change in IVCM imaging may differ from what we observed in our current study. Extending our current study for a longer duration will provide valuable information about chronic neuroinflammatory changes in corneal nerve density and inflammatory cell infiltration.

This study provides a proof-of-concept method to identify the same SNP area of the rat cornea at various time points in vivo. Through the precise detection of detailed morphological changes in SNP, we obtained valuable information on DED progression. By incorporating this technique with μOCT and artificial-intelligence-assisted imaging identification, we can potentially develop a new corneal nerve image acquisition platform for use in the clinical environment.

REFERENCES

1. Lin H, Yiu SC. Dry eye disease: A review of diagnostic approaches and treatments. Saudi J Ophthalmol 2014; 28:173-81. [PMID: 25278793].

2. Yiu SC. Dry eye and ocular surface disease. Saudi J Ophthalmol 2014; 28:163-[PMID: 25278790].

3. Conrady CD, Joos ZP, Patel BCK. Review: The lacrimal gland and its role in dry eye. J Ophthalmol 2016; 2016:7542929[PMID: 27042343].

4. Kojima T, Dogru M, Kawashima M, Nakamura S, Tsubota K. Advances in the diagnosis and treatment of dry eye. Prog Retin Eye Res 2020; xx:100842[PMID: 32004729].

5. Balne PK, Au VB, Tong L, Ghosh A, Agrawal M, Connolly J, Agrawal R. Bead based multiplex assay for analysis of tear cytokine profiles. J Vis Exp 2017; 2017:55993-[PMID: 29053687].

6. Hirayama M. Advances in functional restoration of the Lacrimal Glands. Invest Ophthalmol Vis Sci 2018; 59:DES174-82. [PMID: 30481824].

7. Mansoor H, Ong HS, Riau AK, Stanzel TP, Mehta JS, Yam GH-F. Current Trends and Future Perspective of Mesenchymal Stem Cells and Exosomes in Corneal Diseases. Int J Mol Sci 2019; 20:2853-[PMID: 31212734].

8. Nguyen P, Rue K, Heur M, Yiu SC. Ocular surface rehabilitation: Application of human amniotic membrane in high-risk penetrating keratoplasties. Saudi J Ophthalmol 2014; 28:198-202. [PMID: 25278797].

9. Wilson SL, El Haj AJ, Yang Y. Control of scar tissue formation in the cornea: strategies in clinical and corneal tissue engineering. J Funct Biomater 2012; 3:642-87. [PMID: 24955637].

10. Lagali N, Bourghardt B, Germundsson J, Eden U, Danyali R, Rinaldo M, Fagerholm P. Laser-Scanning in vivo Confocal Microscopy of the Cornea: Imaging and Analysis Methods for Preclinical and Clinical Applications. In: Confocal Laser Microscopy - Principles and Applications in Medicine, Biology, and the Food Sciences. InTech; 2013.

11. Fakih D, Zhao Z, Nicolle P, Reboussin E, Joubert F, Luzu J, Labbé A, Rostène W, Baudouin C, Mélik Parsadaniantz S, Réaux-Le Goazigo A. Chronic dry eye induced corneal hypersensitivity, neuroinflammatory responses, and synaptic plasticity in the mouse trigeminal brainstem. J Neuroinflammation 2019; 16:268-[PMID: 31847868].

12. Simpson F, Alarcon EI, Hilborn J, Brunette I, Griffith M. Regenerative Medicine in the Cornea. Principles of Regenerative Medicine(Third Edition), Academic Press, 2019; 1115–1129.

13. Pedrotti E, Chierego C, Cozzini T, Merz T, Lagali N, De Gregorio A, Fasolo A, Bonacci E, Bonetto J, Marchini G. In Vivo Confocal Microscopy of the Corneal-Conjunctival Transition in the Evaluation of Epithelial Renewal after SLET. J Clin Med 2020; 9:3574-[PMID: 33171960].

14. Stachs O, Guthoff RF, Aumann S. In Vivo Confocal Scanning Laser Microscopy. In: Bille JF, editor. Cham (CH): 2019. p. 263–284.

15. Moein HR, Akhlaq A, Dieckmann G, Abbouda A, Pondelis N, Salem Z, Müller RT, Cruzat A, Cavalcanti BM, Jamali A, Hamrah P. Visualization of microneuromas by using in vivo confocal microscopy: An objective biomarker for the diagnosis of neuropathic corneal pain? Ocul Surf 2020; 18:651-6. [PMID: 32663518].

16. Chirapapaisan C, Abbouda A, Jamali A, Müller RT, Cavalcanti BM, Colon C, Witkin D, Sahin A, Dana R, Cruzat A, Hamrah P. In Vivo Confocal Microscopy Demonstrates Increased Immune Cell Densities in Corneal Graft Rejection Correlating With Signs and Symptoms. Am J Ophthalmol 2019; 203:26-36. [PMID: 30790547].

17. Esquenazi S, He J, Li N, Bazan NG, Esquenazi I, Bazan HEP. Comparative in vivo high-resolution confocal microscopy of corneal epithelium, sub-basal nerves and stromal cells in mice with and without dry eye after photorefractive keratectomy. Clin Exp Ophthalmol 2007; 35:545-9. [PMID: 17760637].

18. Müller LJ, Marfurt CF, Kruse F, Tervo TMT. Corneal nerves: structure, contents and function. Exp Eye Res 2003; 76:521-42. [PMID: 12697417].

19. He J, Bazan NG, Bazan HEP. Mapping the entire human corneal nerve architecture. Exp Eye Res 2010; 91:513-23. [PMID: 20650270].

20. Patel DV, McGhee CNJ. Mapping of the normal human corneal sub-Basal nerve plexus by in vivo laser scanning confocal microscopy. Invest Ophthalmol Vis Sci 2005; 46:4485-8. [PMID: 16303938].

21. Bohn S, Stache N, Sterenczak K, Sperlich K, Allgeier S, Köhler B, Mikut R, Reichert K-M, Guthoff R, Stachs O. Longitudinal evaluation of the subbasal nerve plexus at identical corneal regions by large-area confocal microscopy. In:ARVO Conference;2023;New Orleans, LA, USA. Invest Ophthalmol Vis Sci 2023; 64:4025.

22. Stache N, Sterenczak KA, Sperlich K, Marfurt CF, Allgeier S, Köhler B, Mikut R, Bartschat A, Reichert KM, Guthoff RF, Stachs A, Stachs O, Bohn S. Assessment of dynamic corneal nerve changes using static landmarks by *in vivo* large-area confocal microscopy-a longitudinal proof-of-concept study. Quant Imaging Med Surg 2022; 12:4734-46. [PMID: 36185050].

23. Colorado LH, Edwards K, Chinnery HR, Bazan HE. In vivo immune cell dynamics in the human cornea. Exp Eye Res 2020; 199:108168[PMID: 32846151].

24. Downie LE, Zhang X, Wu M, Karunaratne S, Loi JK, Senthil K, Arshad S, Bertram K, Cunningham AL, Carnt N, Mueller SN, Chinnery HR. Redefining the human corneal immune compartment using dynamic intravital imaging. Proc Natl Acad Sci U S A 2023; 120:e2217795120[PMID: 37487076].

25. Labbé A, Liang Q, Wang Z, Zhang Y, Xu L, Baudouin C, Sun X. Corneal nerve structure and function in patients with non-sjogren dry eye: clinical correlations. Invest Ophthalmol Vis Sci 2013; 54:5144-50. [PMID: 23833066].

26. Wartak A, Schenk MS, Bühler V, Kassumeh SA, Birngruber R, Tearney GJ. Micro-optical coherence tomography for high-resolution morphologic imaging of cellular and nerval corneal micro-structures. Biomed Opt Express 2020; 11:5920-33. [PMID: 33149996].

27. Meng ID, Barton ST, Mecum NE, Kurose M. Corneal sensitivity following lacrimal gland excision in the rat. Invest Ophthalmol Vis Sci 2015; 56:3347-54. [PMID: 26024120].

28. Skrzypecki J, Tomasz H, Karolina C. Variability of Dry Eye Disease Following Removal of Lacrimal Glands in Rats. Adv Exp Med Biol 2019; 1153:109-15. [PMID: 30806916].

29. Chang YA, Wu YY, Lin CT, Kawasumi M, Wu CH, Kao SY, Yang YP, Hsu CC, Hung KF, Sun YC. Animal models of dry eye: Their strengths and limitations for studying human dry eye disease. J Chin Med Assoc 2021; 84:459-64. [PMID: 33871392].

30. McKay TB, Seyed-Razavi Y, Ghezzi CE, Dieckmann G, Nieland TJF, Cairns DM, Pollard RE, Hamrah P, Kaplan DL. Corneal pain and experimental model development. Prog Retin Eye Res 2019; 71:88-113. [PMID: 30453079].

31. Kowtharapu BS, Winter K, Marfurt C, Allgeier S, Köhler B, Hovakimyan M, Stahnke T, Wree A, Stachs O, Guthoff RF. Comparative quantitative assessment of the human corneal sub-basal nerve plexus by in vivo confocal microscopy and histological staining. Eye (Lond) 2017; 31:481-90. [PMID: 27813513].

32. Simsek C, Kojima T, Nagata T, Dogru M, Tsubota K. Changes in murine subbasal corneal nerves after scopolamine-induced dry eye stress exposure. Invest Ophthalmol Vis Sci 2019; 60:615-23. [PMID: 30735229].

33. Carlson EC, Drazba J, Yang X, Perez VL. Visualization and characterization of inflammatory cell recruitment and migration through the corneal stroma in endotoxin-induced keratitis. Invest Ophthalmol Vis Sci 2006; 47:241-8. [PMID: 16384969].

34. Cardigos J, Barcelos F, Carvalho H, Hipólito D, Crisóstomo S, Vaz-Patto J, Alves N. Tear Meniscus and Corneal Sub-basal Nerve Plexus Assessment in Primary Sjögren Syndrome and Sicca Syndrome Patients. Cornea 2019; 38:221-8. [PMID: 30379721].

35. Giannaccare G, Pellegrini M, Sebastiani S, Moscardelli F, Versura P, Campos EC. In vivo confocal microscopy

morphometric analysis of corneal subbasal nerve plexus in dry eye disease using newly developed fully automated system. Graefes Arch Clin Exp Ophthalmol 2019; 257:583-9. [PMID: 30637452].

36. Shetty R, Sethu S, Deshmukh R, Deshpande K, Ghosh A, Agrawal A, Shroff R. Corneal Dendritic Cell Density Is Associated with Subbasal Nerve Plexus Features, Ocular Surface Disease Index, and Serum Vitamin D in Evaporative Dry Eye Disease. Biomed Res Int 2016; 2016:4369750[PMID: 26904676].

37. Villani E, Magnani F, Viola F, Santaniello A, Scorza R, Nucci P, Ratiglia R. In vivo confocal evaluation of the ocular surface morpho-functional unit in dry eye. Optom Vis Sci 2013; 90:576-86. [PMID: 23670123].

38. Choi EY, Kang HG, Lee CH, Yeo A, Noh HM, Gu N, Kim MJ, Song JS, Kim HC, Lee HK. Langerhans cells prevent subbasal nerve damage and upregulate neurotrophic factors in dry eye disease. PLoS One 2017; 12:e0176153[PMID: 28441413].

39. Di Zazzo A, Kheirkhah A, Abud TB, Goyal S, Dana R. Management of high-risk corneal transplantation. Surv Ophthalmol 2017; 62:816-27. [PMID: 28012874].

40. Kobashi H, Kamiya K, Sambe T, Nakagawa R. Factors influencing subjective symptoms in dry eye disease. Int J Ophthalmol 2018; 11:1926-31. [PMID: 30588424].

41. Zhang M, Chen J, Luo L, Xiao Q, Sun M, Liu Z. Altered corneal nerves in aqueous tear deficiency viewed by in vivo confocal microscopy. Cornea 2005; 24:818-24. [PMID: 16160498].